Magnetism in cupric oxide

1988 J. Phys. C: Solid State Phys. 21 2917

(http://iopscience.iop.org/0022-3719/21/15/023)

J. Phys. C: Solid State Phys. **21** (1988) 2917–2929. Printed in the UK

Magnetism in cupric oxide

J B Forsyth†, P J Brown‡ and B M Wanklyn§

† Rutherford Appleton Laboratory, Chilton, Didcot, Oxon OX11 0QX, UK
‡ Institut Laue Langevin, BP 156, 38042 Grenoble Cedex, France
§ Clarendon Laboratory, Parks Road, Oxford OX1 3PU, UK

Received 20 January 1988

Abstract. Single-crystal neutron diffraction measurements have been used to study the long-range magnetic ordering in cupric oxide, CuO. An incommensurate antiferromagnetic structure forms below the Néel temperature of 230(1) K, with a propagation vector $(0.506(1)\boldsymbol{a}^* - 0.483(1)\boldsymbol{c}^*)$ which remains constant down to a magnetic phase transition at 213(1) K. Below the latter temperature, the structure remains antiferromagnetic with a commensurate propagation vector $(\frac{1}{2}\,0\,-\frac{1}{2})$, and this structure persists to the lowest temperature reached in the investigation (20 K). The arrangement of the copper moments in both phases is such that the *n*-glide perpendicular to the ***b*** axis of the monoclinic cell, space group $C2/c$, does not reverse the direction of the spin. The two magnetic sublattices related to the C-face-centring scatter in phase quadrature and the relative directions of the spins on them could not be determined. Good agreement is obtained for the commensurate phase with a multipole model for the copper magnetisation density and spins of 0.65(3) μ_B directed parallel to ***b***. The lower sublattice magnetisation in the incommensurate phase precluded a meaningful multipole fit, but a reasonable agreement is obtained with a model in which the spins rotate in the ***a–c*** plane following an elliptical envelope with major axis directed 33(2)° to ***c*** in β obtuse and a maximum moment of 0.38(2) μ_B at 215 K. The paramagnetic scattering at ambient temperature and 550 K was measured to try to find the origin of the peak in the susceptibility. No significant paramagnetic scattering could be obtained from a powdered sample although the sensitivity of detection was some five times that required to observe the scattering from a Cu^{2+} ion in an ideal paramagnet.

1. Introduction

Cupric oxide, CuO, is unique amongst the monoxides of the 3d transition elements in having a monoclinic unit cell and square planar coordination of copper by oxygen (Tunnell *et al* 1933, 1935), rather than the cubic rock salt structure and octahedral coordination. The temperature dependence of its susceptibility has been measured by O'Keeffe and Stone (1962) and it is also anomalous: instead of the usual Curie–Weiss dependence, the susceptibility exhibits a broad maximum around 550 K (figure 1). At lower temperatures it drops to a value of 2×10^{-6} emu g^{-1}, which is then independent of temperature below 130 K. A specific heat anomaly was found at 220 K by Jih-Heng Hu and Johnston (1953), who associated it with the onset of antiferromagnetism. Until now neutron diffraction data on CuO were limited to a powder study by Brockhouse (1954, 1960).

0022-3719/88/152917 + 13 $02.50

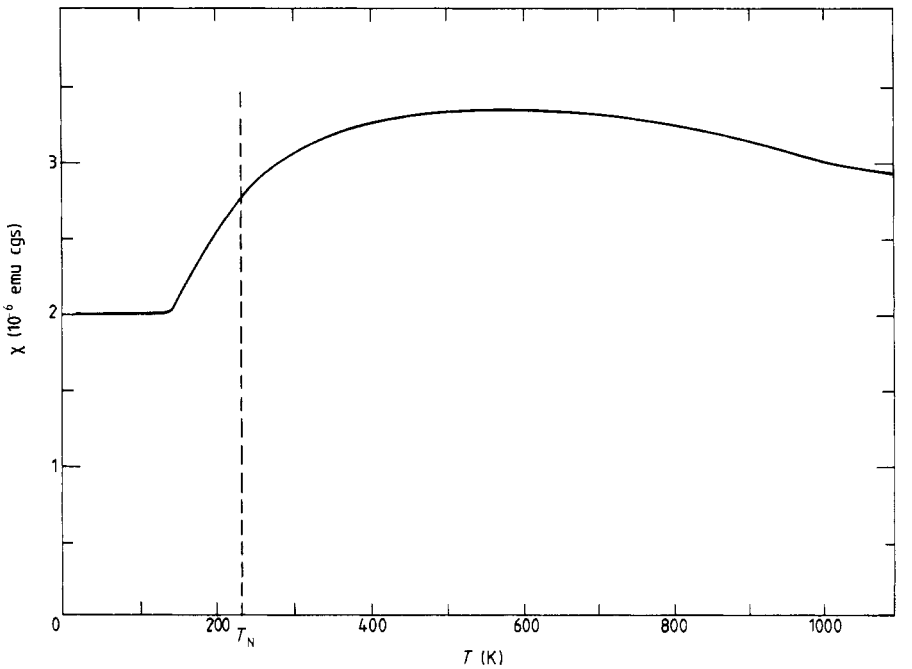

Figure 1. The magnetic susceptibility of CuO, as determined by O'Keeffe and Stone (1962).

In this paper we report a complete determination of the magnetic structures of CuO based on single-crystal neutron diffraction: preliminary results were presented as poster 5PM3 at the *International Conference on Magnetism*, San Francisco, August 1985.

2. Previous structural work on CuO

The crystal structure of CuO was determined by Tunnell *et al* (1933, 1935) using x-ray diffraction. The unit cell is monoclinic, space group $C2/c$; the cell parameters for a natural crystal of tenorite were $a = 4.662$, $b = 3.417$, $c = 5.118$ Å, $\beta = 97°29'$. The structure, which was subsequently refined by Åsbrink and Norrby (1970) from x-ray data, is illustrated in figure 2. The unit cell contains four copper atoms in 4*c* positions ($(\frac{1}{4}\frac{1}{4}0)$ etc) and four oxygen atoms in 4*e* positions ($(0\,y\,\frac{1}{4})$ etc with $y = 0.4184$).

In his powder study of the antiferromagnetic structure of CuO, Brockhouse (1954) found only a single magnetic reflection which he indexed as $(\frac{1}{2}\,0\,-\frac{1}{2})$, but this did not provide sufficient information to determine a complete magnetic structure or the magnitude of the copper moment.

3. Single-crystal neutron scattering in the temperature range 20–213 K

The present study has been carried out on synthetic crystals of CuO prepared by flux growth in a platinum crucible. The starting materials for the flux were MoO_3, V_2O_3 and K_2CO_3, as described by Wanklyn and Garrard (1983).

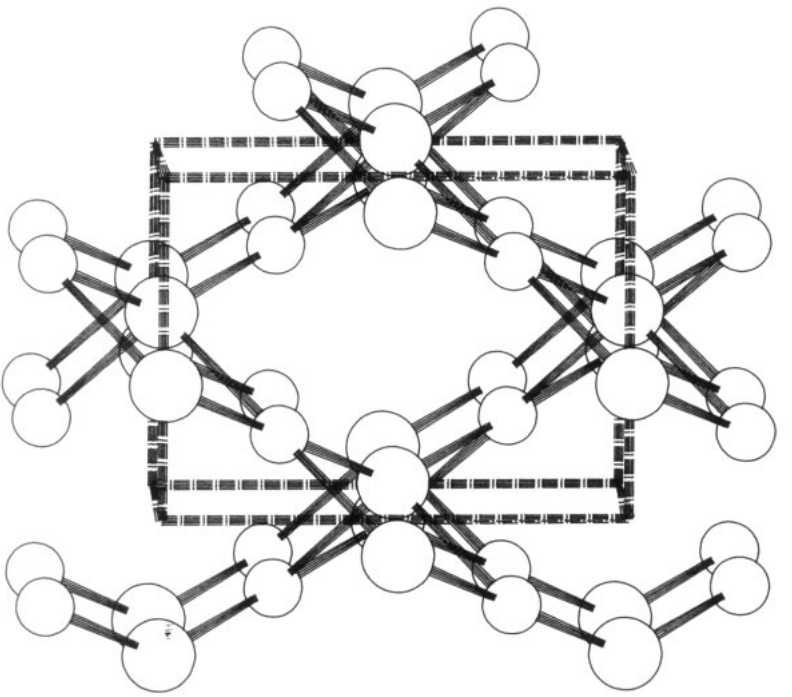

Figure 2. The crystal structure of cupric oxide, CuO. The ribbons formed by the square-planar coordinated Cu atoms linked through the sharing of pairs of oxygen atoms (the larger circles) can clearly be seen.

Initially, neutron diffraction data were collected on the D15 instrument at the Institut Laue Langevin, Grenoble. The diffractometer was fitted with a detector which could be tilted out of the horizontal plane and a vertical liquid helium, variable-temperature cryostat on the central ω axis. The incident wavelength was 1.175 Å. A small 29 mg, single crystal of CuO was mounted in the cryostat with its [010] axis approximately vertical. After cooling to 100 K, well below the Néel point, a preliminary search for magnetic reflections was made and a strong reflection was found with indices $(\frac{1}{2}\,0\,-\frac{1}{2})$. This reflection was indeed the only one found in the earlier powder study by Brockhouse (1954). Its temperature dependence is illustrated in figure 3.

Integrated intensity data were then collected at 20 K. Limited $\{h0l\}$ and $\{h1l\}$ data were first obtained out to a sin Θ/λ limit of 0.43 Å^{-1} at integer and half-integer values of both h and l. They showed that magnetic intensity was confined to reflections in which both h and l were half-integer, but with the additional constraint that $(h + l)$ must be divisible by two. Secondly, the magnetic data were extended to sin $\Theta/\lambda = 0.60$ Å^{-1} and, thirdly, a data set was collected for nuclear reflections out to sin $\Theta/\lambda = 0.74$ Å^{-1}.

Subsequently, a second series of measurements was made on the same single crystal using the D9 diffractometer with a single stage Displex cooler and 4-circle geometry. The lowest temperature was limited to 60 K. A short wavelength of 0.70 Å was used to measure a nuclear data set out to sin $\Theta/\lambda = 0.71$ Å^{-1}, but the crystal reflectivity and the incident flux at this wavelength were not sufficient to give good statistics for the generally

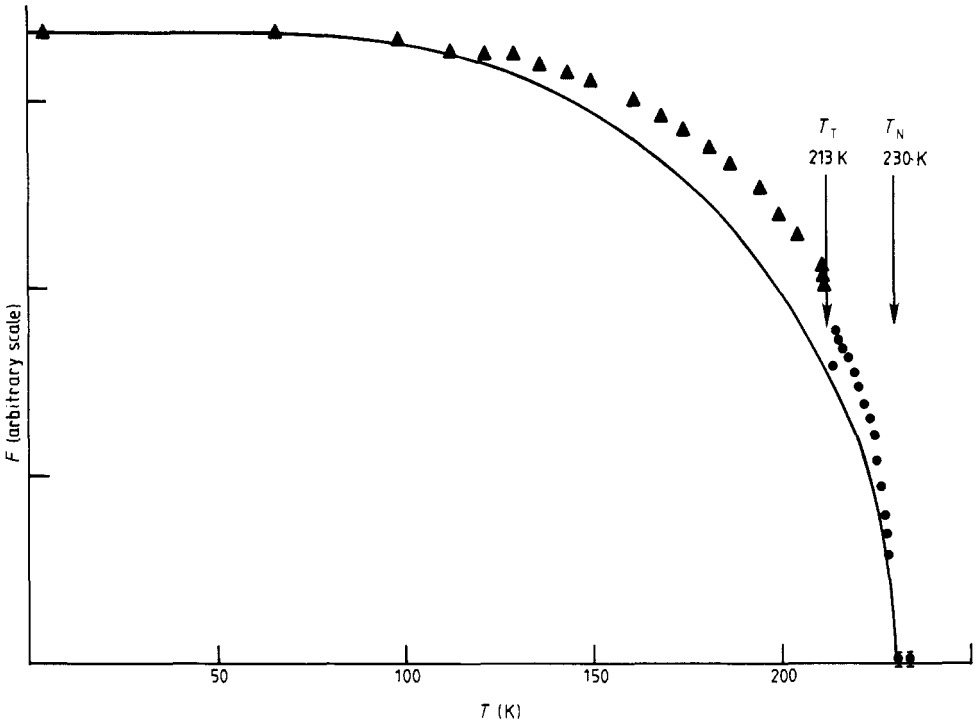

Figure 3. The temperature dependence of the structure factor for the $(\frac{1}{2}\,0\,-\frac{1}{2})$ magnetic reflection in CuO. Above 213 K, the structure factor for the (0.506, 0, −0.483) reflection is shown. The broken curve illustrates the Brillouin function for a spin-$\frac{1}{2}$ ion.

weak magnetic reflections. These were measured at 0.84 Å, together with a few nuclear reflections for intercomparison reasons. The sin Θ/λ limit of these data was 0.50 $Å^{-1}$.

3.1. Nuclear structure

The 57 independent structure amplitudes measured at 20 K and the 131 measured at 60 K were used in a least-squares refinement and the positional and thermal parameters listed in table 1 were obtained. The extinction parameters refer to the Becker and Coppens (1974) Lorentzian model for which the domain radius was fixed at a large value. The extinction was generally small, producing an intensity loss of some 0.6 in the worst case, and it was shown to be negligible for all the magnetic intensities. The crystal parameters are not significantly different from those obtained at room temperature by Åsbrink and Norrby (1970) and also listed in table 1.

3.2. The magnetic structure

The positions of the magnetic reflections define the propagation vector for the magnetic structure as $(\frac{1}{2}\,0\,-\frac{1}{2})$ referred to the chemical cell. The additional condition that $h + l = 2n$ shows that the n-glide plane perpendicular to $\boldsymbol{b}$ does not reverse the spin direction. With the $(\frac{1}{2}\,0\,-\frac{1}{2})$ propagation vector, the phase difference associated with the C-face-

Table 1. Positional, thermal and extinction parameters for CuO, together with their estimated standard deviations; the columns of results are from neutron data collected at 20 and 60 K, from neutron data collected from a second crystal at 195 K, and from the x-ray study of Åsbrink and Norrby (1970). (ITF is the isotropic temperature factor.)

Parameter	Neutron	Neutron	X-ray
Temperature (K)	20–60	195	ambient
a (Å)	4.677(3)	4.681(2)	4.6837(5)
b (Å)	3.423(7)	3.429(1)	3.4226(5)
c (Å)	5.126(3)	5.131(2)	5.1288(6)
β (deg)	99.72(2)	99.63(2)	99.54(1)
Cu ITF (Å^2)	0.16(2)	0.41(4)	anisotropic
0 y	0.4188(3)	0.4194(5)	0.4184(13)
0 ITF (Å^2)	0.28(2)	0.51(4)	anisotropic
Mosaic	0.074(4)	0.063(6)	
R-factor	0.025	0.031	0.032

centring translation is $\pi/2$. The two magnetic sub-lattices related by this translation therefore scatter in phase quadrature, so that the relative directions of the spins on sublattices cannot be determined from intensity measurements. Figure 4 illustrates the magnetic arrangement in several adjacent unit cells.

Amongst the possible spin arrangements consistent with both the chemical cell symmetry and the magnetic model are a simple collinear structure with spins either in the ***a–c*** plane or along the ***b*** direction, or a spiral structure with the spins confined to the ***a–c*** plane. To distinguish between different models, account must be taken of the intensities of the observed magnetic reflections. The magnetic intensity data measured

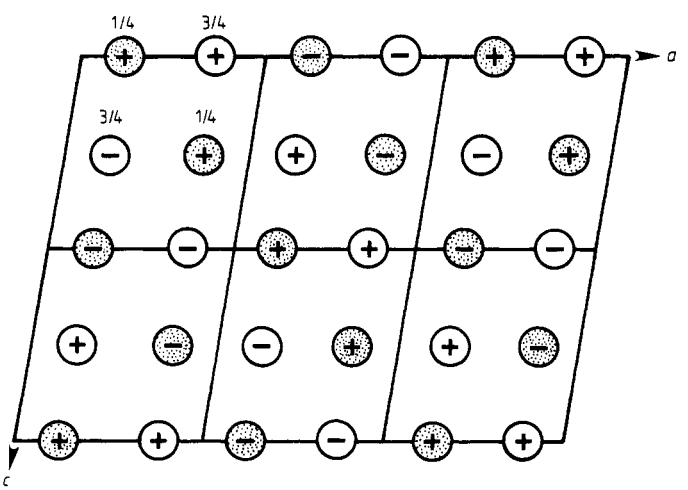

Figure 4. The low-temperature magnetic arrangement in several adjacent cells of CuO. Ions on the two sublattices related by the C-centring are differentiated by open and stippled circles.

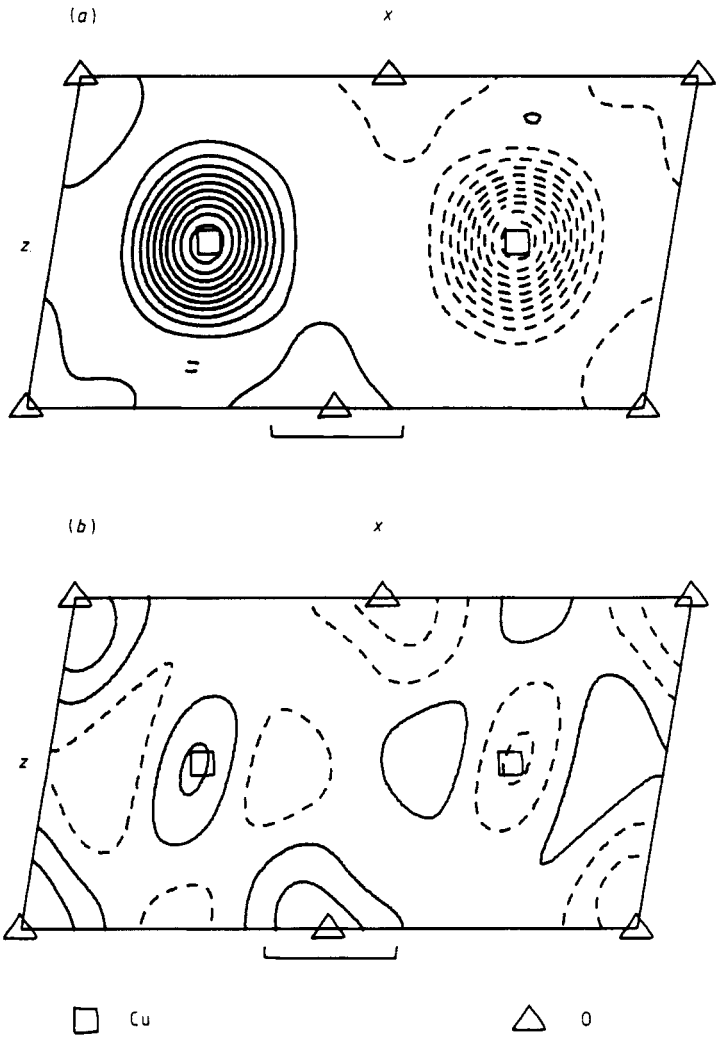

Figure 5. (*a*) The [010] Fourier projection of the observed magnetisation in CuO in its commensurate phase. (*b*) The [010] difference density from a model calculation based on a spherically symmetric copper moment. The scale bar represents 1 Å.

at 20 and 60 K were scaled together and placed on an absolute scale by reference to the nuclear intensities measured at the lower temperature. Least-squares fits to the 59 independent structure amplitudes were made for the arrangement shown in figure 4, a Cu^{2+} free-ion form factor derived from the wavefunctions of Clementi and Roetti (1974) and various spin directions. Although the goodness-of-fit showed that the ***b*** axis moment model was clearly preferred, the agreement between this model and the observed data ($R = 0.16$) and the large value for χ^2 (139) suggested that the model might be further refined. A feature of all models was the tendency of the calculated moduli of structure factors to fall off more rapidly with increasing $\sin\Theta/\lambda$ than the observations. Figure

Table 2. Observed moduli of magnetic structure factors, F_0, for the commensurate phase of CuO (together with their standard deviations) and those calculated, F_c, for a model with a ***b*** axis spin direction and the multipole coefficients for the moments given in table 3.

h	k	l	$\|F_0\|$	F_c	F_0-F_c
-4.5	0.0	0.5	0.598(32)	0.5631	0.0351
-2.5	0.0	0.5	0.877(11)	-0.9151	-0.0386
-0.5	0.0	0.5	1.5788(90)	1.5918	-0.0130
1.5	0.0	0.5	1.0824(59)	-1.0976	-0.0152
3.5	0.0	0.5	0.754(15)	0.8081	-0.0539
-4.5	1.0	0.5	0.410(42)	0.4339	-0.0236
-2.5	1.0	0.5	0.8302(94)	-0.8987	-0.0685
-0.5	1.0	0.5	0.518(21)	0.4545	0.0637
1.5	1.0	0.5	0.975(21)	-0.9910	-0.0161
3.5	1.0	0.5	0.584(15)	0.6150	-0.0310
-2.5	2.0	0.5	0.551(30)	0.4980	0.0529
-0.5	2.0	0.5	0.236(73)	-0.2156	0.0205
1.5	2.0	0.5	0.495(19)	0.4704	0.0243
3.5	2.0	0.5	0.393(60)	-0.4490	-0.0556
1.5	3.0	0.5	0.233(75)	0.2373	-0.0041
-5.5	0.0	1.5	0.240(79)	-0.3381	-0.0981
-3.5	0.0	1.5	0.636(14)	0.6209	0.0153
-1.5	0.0	1.5	1.3080(86)	-1.2646	0.0434
0.5	0.0	1.5	1.0620(50)	1.0847	-0.0227
2.5	0.0	1.5	0.9533(84)	-0.9697	-0.0164
4.5	0.0	1.5	0.501(49)	0.4589	0.0419
-3.5	1.0	1.5	0.648(16)	-0.5663	0.0821
-1.5	1.0	1.5	0.773(20)	0.8513	-0.0783
0.5	1.0	1.5	0.899(11)	-0.8304	0.0687
2.5	1.0	1.5	0.7657(95)	0.7837	-0.0180
4.5	1.0	1.5	0.503(75)	-0.4297	0.0735
-3.5	2.0	1.5	0.462(45)	-0.3914	0.0706
-1.5	2.0	1.5	0.492(22)	0.4458	0.0461
0.5	2.0	1.5	0.448(23)	-0.4330	0.0152
2.5	2.0	1.5	0.478(35)	0.5005	-0.0225
-1.5	3.0	1.5	0.355(62)	-0.2102	0.1452
0.5	3.0	1.5	0.300(91)	0.2181	0.0820
-4.5	0.0	2.5	0.301(43)	0.3560	-0.0552
-2.5	0.0	2.5	1.036(54)	-0.8116	0.2243
-0.5	0.0	2.5	0.8351(87)	0.8974	-0.0623
1.5	0.0	2.5	0.9579(96)	-0.9472	0.0107
3.5	0.0	2.5	0.515(23)	0.5334	-0.0182
-2.5	1.0	2.5	0.644(15)	-0.5507	0.0936
-0.5	1.0	2.5	0.8101(78)	0.8469	-0.0368
1.5	1.0	2.5	0.734(11)	-0.7095	0.0249
3.5	1.0	2.5	0.538(32)	0.5175	0.0203
-2.5	2.0	2.5	0.41(11)	0.3841	0.0231
-0.5	2.0	2.5	0.530(24)	-0.4506	0.0798
1.5	2.0	2.5	0.474(25)	0.4835	-0.0094
-3.5	0.0	3.5	0.422(25)	0.4500	-0.0276
-1.5	0.0	3.5	0.607(13)	-0.6078	-0.0005
0.5	0.0	3.5	0.688(12)	0.7566	-0.0683
2.5	0.0	3.5	0.493(23)	-0.5214	-0.0287
-3.5	1.0	3.5	0.287(37)	-0.3634	-0.0769
-1.5	1.0	3.5	0.621(11)	0.5411	0.0801
0.5	1.0	3.5	0.523(14)	-0.6252	-0.1026
2.5	1.0	3.5	0.481(24)	0.4832	-0.0027
-1.5	2.0	3.5	0.427(45)	0.3610	0.0657
0.5	2.0	3.5	0.437(44)	-0.4088	0.0280
-2.5	0.0	4.5	0.365(32)	-0.3472	0.0177
-0.5	0.0	4.5	0.459(28)	0.5090	-0.0496
1.5	0.0	4.5	0.310(75)	-0.4291	-0.1189
-2.5	1.0	4.5	0.278(41)	-0.3423	-0.0638
-0.5	1.0	4.5	0.394(30)	0.4116	-0.0179

5(*a*) shows the observed [010] Fourier projection of the magnetisation and figure 5(*b*) illustrates the difference density from the model calculation based on a spherically symmetric copper moment with an expanded form factor. The latter figure shows that the copper moment is elongated in projection and the some small moment is associated with the oxygen sites.

A multipole refinement of the moment distribution on the Cu site improved the R-factor to 0.11 and a similar treatment of both the copper and oxygen moments produced a good fit with $R = 0.076$ and $\chi^2 = 9$. Table 2 lists the observed moduli of the magnetic structure factors, together with their estimated errors and those calculated for this model. Figure 6(*a*) illustrates the difference density between the new model and the previous, simpler one and it can be seen to reproduce the significant features of figure

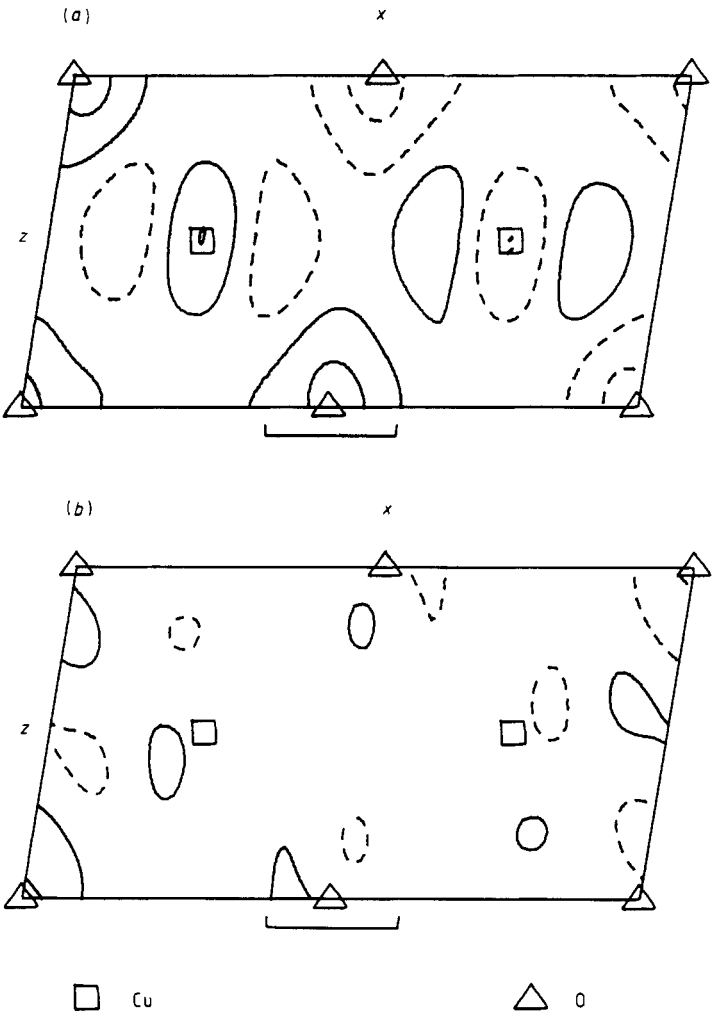

Figure 6. (*a*) The [010] Fourier projection of the calculated difference density between the multipole model and that based on the simple spherically symmetric copper moment. (*b*) The final [010] projected difference density between the observed magnetisation and the multipole model whose coefficients are given in table 3. The scale bar represents 1 Å.

5(*b*). The final difference [010] projection density is shown in figure 6(*b*) and the multipole coefficients of the final model are given in table 3.

4. The magnetic structure in the temperature range 213–230 K

Although the intensity of the magnetic reflection ($\frac{1}{2}\,0\,-\frac{1}{2}$) disappears abruptly at 213 K (figure 3), some 17 K below the Néel temperature reported by Brockhouse (1954), measurement of the ($\frac{3}{2}\,0\,\frac{1}{2}$) reflection showed that, above the transition temperature of

Table 3. Multipole coefficients for the copper moment in the low-temperature antiferromagnetic phase of CuO. The coefficients of the copper hexadecapoles and the oxygen quadrupoles are not significantly determined and the exclusion of these multipoles does not significantly worsen the agreement factor $R = 0.074$ or $\chi^2 = 8.9$.

Atom	Multipole	Coefficient
Cu	Y_{00}	0.654(28)
	Y_{20}	−0.103(38)
	Y_{22}	0.199(56)
	Y_{40}	0.009(140)
	Y_{42}	−0.020(195)
	Y_{44}	−0.090(192)
O	Y_{00}	0.144(36)
	Y_{20}	0.062(48)
	Y_{22}	0.032(40)

213 K, a new peak appeared somewhat shifted from the centre of the scan. Using the D15 diffractometer and a small detector aperture, the centres of a number of these satellite peaks were determined at 215 K. With the specimen mounted about [010], only one satellite reflection was found close to each reflection of the commensurate magnetic phase and the mean displacement determined from the positions of the centred peaks was consistent with a propagation vector $\boldsymbol{\tau} = 0.506(1)\boldsymbol{a}^* - 0.483(1)\boldsymbol{c}^*$. No satellite reflections were found associated with possible antiferromagnetic reflections not obeying the rule $h + l = 2n$, from which it can be concluded that, as in the commensurate structure, copper atoms related by the n-glide plane have parallel spins.

The temperature dependences of the position and integrated intensity of the $(0.506, 0, -0.483)$ reflection were measured between 213 and 230 K. No change in the position of the reflection was observed, showing that the propagation vector is temperature independent. The variation of the intensity is also illustrated in figure 3, from which it can be seen that the Néel temperature is 230 K in good agreement with the early powder experiment.

The integrated intensities of the satellites were measured at 215 K using both the 29 mg specimen mounted about [010] and a second 38 mg specimen mounted about [001]. The 37 independent magnetic structure amplitudes, obtained by merging the data sets from the two specimens using a scale factor deduced from refinements of the two associated nuclear data sets, were used in least-squares fits to determine the parameters associated with the three possibilities for the orientation of the moments described in § 3.2 for the commensurate phase. These parameters are reported in table 4 together with the goodness of fit. The best fit for a spherically symmetric copper moment was obtained with the moments in the $\boldsymbol{a}$–$\boldsymbol{c}$ plane with their magnitude and directions given by a function of the form

$$\boldsymbol{S} = \boldsymbol{S}_{\parallel} \cos 2\pi(\boldsymbol{\tau} \cdot \boldsymbol{R}) + \boldsymbol{S}_{\perp} \sin 2\pi(\boldsymbol{\tau} \cdot \boldsymbol{R})$$

where $\boldsymbol{R}$ is any lattice vector and $\boldsymbol{S}_{\parallel}$ and $\boldsymbol{S}_{\perp}$ are perpendicular vectors in the $\boldsymbol{a}$–$\boldsymbol{c}$ plane. The agreement between this model and the data is not very good ($R = 0.17$), being similar to that found for the simple spherical copper moment calculation for the commensurate phase. The arrangement of magnetic moments in the incommensurate phase is illustrated in figure 7.

Table 4. The parameters and goodness of fit of various models for the incommensurate antiferromagnetic phase of CuO. All models are based on the commensurate phase and on a spiral or amplitude modulated spin density wave whose z axis is held parallel to $\boldsymbol{b}$ by symmetry. The major and minor axes of the spiral envelope are parallel to x and y respectively, and they lie in the $\boldsymbol{a}$–$\boldsymbol{c}$ plane with x making an angle α with $\boldsymbol{c}$ in β acute. Models 5 and 6 are equivalent to 3 and 4 except that the expanded Cu form factor was used in the fit. Although the conventional R-factor remains relatively poor for all models, the goodness of fit is significantly better with models 4 and 6 which corresponds to the elliptical spiral.

Model	S_x	S_y	S_z	α	R-factor	χ^2
1	0.0	0.0	0.248(10)		29.7	182
2	0.316(11)	0.316	0.0		21.4	152
3	0.404(15)	0.0	0.0	33.3(1.7)	21.6	142
4	0.379(13)	0.190(18)	0.0	33.0(2.4)	17.0	76
5	0.365(12)	0.177(18)	0.0	33.6(2.4)	17.3	77
6	0.388(14)	0.0	0.0	33.6(1.6)	21.2	139

A calculation based on the actual density distribution found for the commensurate phase and modelled by the multipole parameters given in table 3 did not refine as well as the simple model ($R = 0.22$) and suggested an even more elliptical envelope for the spins in the $\boldsymbol{a}$–$\boldsymbol{c}$ plane, though with the same direction (within the standard deviations) for the major component. It was therefore considered that the lower precision achieved for the weaker, highly temperature-dependent magnetic intensities measured for the incommensurate phase did not warrant further refinement of the model to include aspherical density and an oxygen moment, though we may conclude that the elliptical

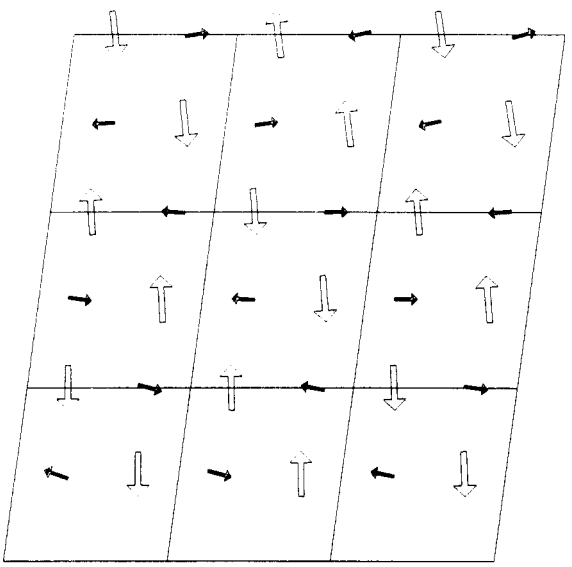

Figure 7. Arrangement of moments in the incommensurate antiferromagnetic phase of CuO. The [010] projection covers several chemical unit cells.

envelope found for the spins is not an artefact arising from the neglect of an asphericity in the Cu moment distribution.

5. The paramagnetic region

In an attempt to understand the anomalous behaviour of the magnetic susceptibility of CuO above T_N (figure 1), we also measured the magnetic diffuse scattering from a 10 cm^{-3} cylindrical powdered sample in the paramagnetic region at ambient and at 550 K, the latter temperature corresponding to the maximum in the observed susceptibility. The measurements were made on the D5 diffractometer at the ILL, using a polarised incident beam of 0.84 Å neutrons and polarisation analysis of the scattered beam to determine the difference in the spin–flip scattering between neutrons polarised parallel and perpendicular to the scattering vector. This technique permits a clean, isothermal separation between magnetic and other sources of scattering (Ziebeck and Brown 1980).

Unexpectedly, no significant paramagnetic scattering was observed at either temperature in a Q-range between 0.9 and 2.2 $Å^{-1}$. The sensitivity of detection was some five times greater than that required to observe the scattering from 1 μ_B/Cu^{2+} ion in an ideal paramagnet. However, the reduced ordered moment of 0.65 μ_B observed in the low-temperature phase would lower the expected paramagnetic intensity to within a factor of two of our estimated level of detection.

6. Discussion

The cupric ion in copper oxide is coordinated by four oxygen atoms in an approximately square planar array. The coordinating squares share one pair of opposite edges to form ribbons running along the ⟨110⟩ directions and lying approximately in the {301} planes (figure 2). Alternating copper atoms within the ribbons belong to the two different sublattices related by the C-face centring. Each oxygen atom is common to two different ribbons related by the axis on which it lies and is bonded to four copper atoms.

In the structure determined for the commensurate phase of CuO the principal magnetic interactions seem to occur between copper atoms on adjacent ribbons. The longer of the two near-neighbour distances (3.74 Å) is associated with antiferromagnetic coupling, through a copper–oxygen–copper bond with a bond angle of 146°. The shorter copper–copper distance (3.19 Å) associated with the sharper bond angle of 109° gives rise to a ferromagnetic interaction. Assuming that these two interactions are dominant, then the connectivity of the structure leads to frustration of the magnetic interactions between near-neighbour copper atoms in the ribbons. Since of the four copper neighbours of each oxygen, one pair is coupled ferromagnetically and the other antiferromagnetically, whichever phase is chosen between the two C-face-centre related sublattices, every oxygen is bonded to three copper atoms with parallel moments and one with an antiparallel moment direction. The direction of the small oxygen moment is parallel to the direction of the ferromagnetically coupled copper pair.

In the incommensurate phase the principal magnetic interactions remain essentially unchanged, but the transition to the incommensurate spiral structure with the spins in the a–c plane slightly relieves frustration in the interaction within the ribbons, which then shows a tendency to be ferromagnetic. It is perhaps unexpected to find a helimagnetic phase condensing from the paramagnetic phase at T_N in a system with monoclinic symmetry since from the theory of second-order transitions (Rossat-Mignod 1987)

a linearly modulated phase might be expected. However in the incommensurate phase of CuO the representation of the helimagnetic order parameter is not two-dimensional, but is represented by two equivalent one-dimensional representations, the two corresponding components of magnetisation being orthogonal in both direction and phase.

The multipole coefficients in table 3 refer to normalised spherical harmonics and it can be seen that our data are only sufficient to define Y_{00}, Y_{20} and Y_{22} with any certainty: this is probably due to its sin Θ/λ limit which occurs before the maximum in the $\langle j_4 \rangle$ radial distribution function associated with the hexadecapoles. The quantum axes for the Cu atom at $(\frac{1}{4}\,\frac{1}{4}\,0)$ were defined with Z perpendicular to the plane of oxygen coordination and X directed to its oxygen neighbour at $(0\ y\ \frac{1}{4})$. Although the accepted orbital scheme for Cu^{2+} in an orthorhombic environment is with the E_g hole states lower and the single hole in a $d_{x^2-y^2}$ orbital pointing towards the ligand ions, no single d state would produce the observed multipoles on these axes. The sign of the Y_{20} multipole is consistent with the occupation of $d_{x^2-y^2}$ rather than d_{z^2}, but the significant positive value for Y_{22} implies that the d_{xz} orbital is also more occupied than d_{yz}. The numerical coefficients are consistent with equal occupation of the $d_{x^2-y^2}$ and d_{xz} orbitals. The only significant multipole required to model the oxygen moment is Y_{00} with a coefficient corresponding to 0.14(4) μ_B parallel to the moment on the majority of its copper neighbours. The remaining parameter in the model corresponds to the modification of the $\langle j_0 \rangle$ radial form factor on copper by the addition of a $\langle j_2 \rangle$ contribution. Its effect, in the range of sin Θ/λ of interest, is to expand the form factor by some 9% corresponding to a contraction of the moment distribution in real space. A similar effect, a form factor expansion of 7%, was found by Umebayashi *et al* (1968) in their study of Cu^{2+} in $CuCl_2 . 2D_2O$.

The temperature dependence of the magnetic reflections $(\frac{1}{2}\,0\,-\frac{1}{2})$ and $(\frac{3}{2}\,0\,\frac{1}{2})$ show no discontinuities on traversing the temperature of 140 K. These data are, however, insufficient for us to suggest any structural reason for the abrupt change in the slope of the temperature dependence of the susceptibility at this temperature (figure 1).

The current explosion of interest in the role of the copper–oxygen sheets in high-temperature superconductors such as $YBa_2Cu_3O_{7-x}$ leads us to suggest that CuO is worthy of further study. We have shown that it is far from being a simple ionic antiferromagnet and have been able to come to some conclusions about its ground-state magnetic wavefunctions. These should be further quantified by a study of the magnetic reflections to a higher value in sin Θ/λ; although these would be very weak, it is unlikely that equivalent information could be obtained from the lower magnetisation densities observed in more structurally related phases such as $YBa_2Cu_3O_{6+x}$ and La_2CuO_3 (Tranquada *et al* 1988, Vaknin *et al* 1987).

We have recently learnt of some measurements of the specific heat of yttrium barium copper oxide materials by Loram *et al* (1988). In addition to the anomaly associated with the 90 K transition to the superconducting state, two further peaks were observed at 212(1) and 229(1) K. Loran and co-workers associated the 229 K peak with the presence of CuO in their samples and measurements were then made on pure CuO which confirmed the existence of both peaks. We can now identify the lower-temperature anomaly with the spin rearrangement at 213(1) K reported above.

References

Åsbrink S and Norrby L-J 1970 *Acta Crystallogr.* B **26** 8
Becker P J and Coppens P 1974 *Acta Crystallogr.* A **30** 129

Brockhouse B N 1954 *Phys. Rev.* **94** 781
—— 1960 *Atomic Energy of Canada Limited Report* CRNP 970
Clementi E and Roetti C 1974 *At. Data Nucl. Data Tables* **14** 177
Jih-Heng Hu and Johnston H L 1953 *J. Am. Chem. Soc.* **75** 2471
Loram J W, Mirza K A, Osborn J and Meisels R 1988 private communication
O'Keeffe M and Stone F S 1962 *J. Phys. Chem. Solids* **23** 261
Rossat-Mignod J 1987 *Methods of Experimental Physics* vol 3, part C (New York: Academic) pp 69–157
Tranquada J M, Cox D E, Kunnmann W, Moudden H, Shirane G, Suenaga M, Zolliker P, Vaknin D, Sinha S K, Alvarez M S, Jacobson A J and Johnston D C 1988 *Phys. Rev. Lett.* **60** 156
Tunnell G, Posnjak E and Ksanda C J 1933 *J. Wash. Acad. Sci.* **23** 195
—— 1935 *Z. Kristallogr.* **90** 120
Umebayashi H, Frazer B C, Cox D E and Shirane G 1968 *Phys. Rev.* **167** 519
Vaknin D, Sinha S K, Moncton D E, Johnston D C, Newsam J M, Safinya C R and King Jr H E 1987 *Phys. Rev. Lett.* **58** 2802
Wanklyn B M and Garrard B J 1983 *J. Mater. Sci. Lett.* **2** 285
Ziebeck K R A and Brown P J 1980 *J. Phys. F: Met. Phys.* **10** 2015